

# GMT: A Robust Global Association Model for Multi-Target Multi-Camera Tracking

Huijie Fan  *Member, IEEE*, Tinghui Zhao , Qiang Wang , Baojie Fan , Yandong Tang  *Member, IEEE*, and LianQing Liu  *Senior Member, IEEE*

**Abstract**—In the task of multi-target multi-camera (MTMC) tracking of pedestrians, the data association problem is a key issue and main challenge, especially with complications arising from camera movements, lighting variations, and obstructions. However, most MTMC models adopt two-step approaches, thus heavily depending on the results of the first-step tracking in practical applications. Moreover, the same targets crossing different cameras may exhibit significant appearance variations, which further increases the difficulty of cross-camera matching. To address the aforementioned issues, we propose a global online MTMC tracking model that addresses the dependency on the first tracking stage in two-step methods and enhances cross-camera matching. Specifically, we propose a transformer-based global MTMC association module to explore target associations across different cameras and frames, generating global trajectories directly. Additionally, to integrate the appearance and spatio-temporal features of targets, we propose a feature extraction and fusion module for MTMC tracking. This module enhances feature representation and establishes correlations between the features of targets across multiple cameras. To accommodate high scene diversity and complex lighting condition variations, we have established the VisionTrack dataset, which enables the development of models that are more generalized and robust to various environments. Our model demonstrates significant improvements over comparison methods on the VisionTrack dataset and others.

**Index Terms**—MTMC tracking, MTMC dataset, vision transformer.

## I. INTRODUCTION

**M**ULTI-TARGET multi-camera (MTMC) tracking [1] has vast applications in numerous domains such as video surveillance [2]–[4], autonomous driving [5], human-computer interaction [6], anomaly action detection [7], crowd

Manuscript received xx xx, xxxx; revised xx xx, xxxx; accepted xx xx, xxxx. Date of publication xx xx, xxxx; date of current version xx xx, xxxx. This work is supported by the National Natural Science Foundation of China (62273339, 62073205, U20A20200). The associate editor coordinating the review of this manuscript and approving it for publication was Prof. xxxx (*Corresponding author: Qiang Wang*).

Huijie Fan, Yandong Tang and LianQing Liu are with the State Key Laboratory of Robotics, Shenyang Institute of Automation, Chinese Academy of Sciences, Shenyang 110016, China (e-mail: fanhuijie@sia.cn; ytang@sia.cn; lqliu@sia.cn).

Tinghui Zhao is with the State Key Laboratory of Robotics, Shenyang Institute of Automation, Chinese Academy of Sciences, Shenyang 110016, China and also with the University of Chinese Academy of Sciences, Beijing 100049, China (e-mail: zhaotinghui@sia.cn).

Qiang Wang is with the Key Laboratory of Manufacturing Industrial Integrated, Shenyang University (e-mail: wangqiang@sia.cn).

Baojie Fan is with the Automation and AI College, Nanjing University of Posts and Telecommunications, Nanjing 210049, China, and also with the State Key Laboratory of Integrated Services Networks, Xi’an 710071, China (e-mail: jobfbj@gmail.com).

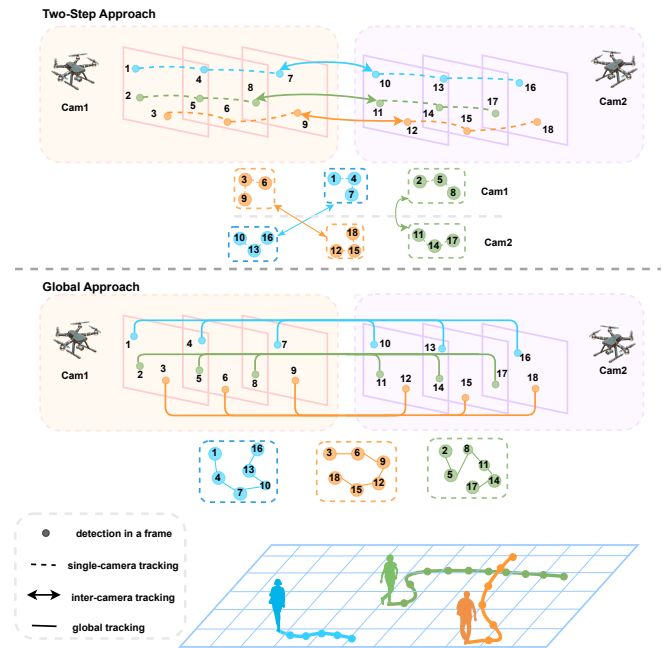


Fig. 1. Two-Step Approach Versus Global Approach in MTMC. Most two-step approaches employ off-the-shelf models for single-camera tracking, followed by inter-camera tracking models. Our global model merges these two steps, associating all targets across cameras and generating global trajectories at once.

behavior analysis [8], [9], and understanding of traffic scenes [10]. Compared to single-camera tracking, multi-camera tracking uses information from cameras at various locations to enhance system robustness and alleviate occlusion issues by offering multiple viewing angles, ensuring more continuous and accurate tracking [11], [12]. However, the appearance, lighting, and background information of one object captured by different cameras usually vary significantly [13], [14], increasing the difficulty of target association in multi-camera tracking.

Most MTMC tracking models proposed in recent years employ two-step approaches, which involves single-camera tracking followed by inter-camera re-identification (Re-ID) (shown in Figure 1, two-step approach). Firstly, single-camera tracking models, such as DeepSORT [15] or FairMOT [16], are used to associate targets across frames within one camera, generating local trajectories. Secondly, Re-ID models [13], [17] are employed to link these local trajectories, creating complete trajectories across multiple cameras. Although this method of target association is widely used, the performance of inter-camera tracking in the second step is greatly influenced

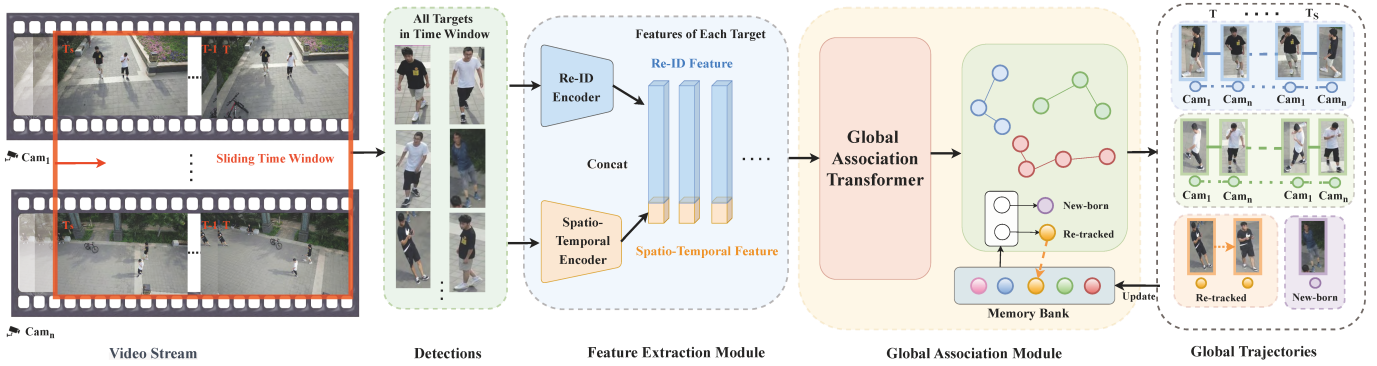


Fig. 2. Our proposed GMT model for MTMC tracking. Our GMT model consists of three main modules. (1) Object Detection Module detects targets frame-by-frame within the video stream. (2) Feature Extraction Module extracts and fuses Re-ID and spatio-temporal features for each target. (3) Global Association Module employs a transformer to produce similarity matrix for target association and engages a memory bank for secondary associating to recover lost trajectories of unmatched targets, ultimately creating global trajectories.

by false positives and trajectory fragments produced by the single-camera tracking in the first step [18]. Furthermore, the two-step approach inherently separates the tracking and Re-ID processes, preventing the model from leveraging the full context of the multi-camera setup during both steps. This separation can result in the loss of valuable temporal and spatial information that could be used to improve tracking accuracy.

Global MTMC tracking models integrate both steps into a unified process (shown in Figure 1, global approach), reducing inaccuracies and enhancing the robustness of target association. Existing global MTMC tracking models are mostly based on constructing a graph which connects targets across all cameras [19], [20]. Global MTMC tracking methods are more robust compared to the two-step MTMC approaches, but they have higher computational complexity and lack real-time capabilities. These models also require sophisticated algorithms to handle the optimization of the global graph.

For a more efficient solution to target association in MTMC tracking, we propose a transformer-based global MTMC tracking model. As shown in Figure 2, this model directly generates global trajectories across cameras from initial detections. Our model simplifies the two-step approach and avoids the complex graph optimization process. With the transformer’s global association capabilities, our model processes all target features within a time window, enabling interaction and enhancement of target features across different cameras, and generating a similarity matrix between targets. Global trajectories for each target are constructed by processing the similarity matrix and using the Hungarian algorithm.

Our model also addresses the limitation of existing MTMC tracking models, which often focus solely on appearance features when associating targets across cameras, by introducing a fused feature representation module that integrates Re-ID features with spatio-temporal features. This integration considers both appearance similarities and the continuity of target trajectories within time windows. The inclusion of spatial-temporal information allows for more robust and accurate target association, as it leverages both visual distinctiveness and movement patterns, leading to improved MTMC tracking performance. To recover the lost trajectories, we introduces

a memory bank module to preserve the historical features of each trajectory. Our end-to-end trainable model achieved competitive performance in six diverse MTMC tracking datasets.

The main contributions are summarized as follows:

- We propose a transformer-based global MTMC tracking model that associates features of targets across different cameras and frames, directly generates global trajectories, and possesses the capability to recover lost trajectories.
- We propose a feature representation module for MTMC tracking, which integrates the appearance and spatio-temporal features of targets to enhance their feature representation, thereby effectively establishing correlations between features of targets in multiple cameras.
- We have established the VisionTrack dataset, a large-scale MTMC tracking dataset featuring high scene diversity and complex lighting condition variations, enabling the development of models that are more generalized and robust to various environments.
- On the VisionTrack dataset, we attained a score of 76.0 in CVMA (Cross-View Matching Accuracy) and 81.4 in CVIDF1 (Cross-View IDF1 Score), outperforming the second-best model by 5.9 in CVMA and 13.0 in CVIDF1.

## II. RELATED WORK

1) *Object Detection*: Object detection is one of the fundamental tasks in computer vision, with the mission of locating and classifying targets of specific categories within images. In recent years, object detection methods can be categorized into anchor-based and anchor-free detection algorithms. Examples of anchor-based algorithms are Faster RCNN [21], SSD [22], and YOLOv2 [23], whereas anchor-free algorithms include YOLO [24], CenterNet [25], and DETR [26]. Our work focuses on feature association between targets, thus we employ CenterNet to detect targets in every frame of the video. Other detection algorithms can also replace CenterNet within our framework.

2) *Two-Step MTMC Tracking*: Two-step MTMC tracking approaches decompose MTMC tracking into two consecutive steps: Single-Camera Tracking (SCT) [27]–[31] and Inter-Camera Tracking (ICT) [32]–[38]. SCT methods include tracking-by-detection paradigm-based DeepSORT [15],



Fig. 3. Examples of the VisionTrack dataset. Our dataset was captured in various weather conditions, times, and scenes. The images from left to right are examples taken during sunny, overcast, dusk, and night-time conditions. The same targets appearing in different cameras are marked with the same colored bounding boxes.

BYTETRACK [39], GTR [40] and joint detection-tracking paradigm-based FairMOT [16]. ICT aims to associate the same targets across different cameras, thereby forming inter-camera trajectories. Inter-camera target Re-ID is a challenging task because the same targets may have different postures, lighting, and occlusions in different cameras. To better perform ICT, some models focus on optimizing and improving target association methods. DyGLIP [41] employs dynamic graphs for link prediction, combining with attention mechanisms to establish accurate data associations among targets. TRACTA [42] formulates the MTMC data association problem as a trajectory-to-target assignment issue, proposing a restricted non-negative matrix factorization algorithm to calculate the assignment matrix. MvMHAT [43] introduces a self-supervised learning framework, establishing pairwise similarity and triplet transitive similarity for learning data association models in MTMC tracking. MIA-NET [44], designed to address the challenges of multi-camera small object tracking, introduces an inter-camera matching model that employs keypoint mapping. Additionally, some models focus on optimizing the feature representation of targets, making the feature more discriminative across different cameras. Crossmot [45] introduces both single-view Re-ID embeddings and cross-view Re-ID embeddings, representing target features distinctively in the two tracking steps. Li et al. [46] proposed intra-tracklet and inter-tracklet attention modules, separately learning each target’s motion and appearance features and each trajectory’s feature representation. Cheng et al. [47] presented a graph model that initially connects detected objects across different cameras spatially, and then transforms these connections into a temporal graph for temporal association.

3) *Global MTMC Tracking*: Existing global MTMC tracking algorithms are most based on graph networks to establish relationship among targets, directly outputting global trajectories. Chen et al. [19] proposed a global graph network that merges SCT and ICT processes. They also introduced a new similarity measurement scheme that balances different similarities in two steps. Liu et al. [20] proposed a method using generalized maximum clique optimization to construct a global graph. Furthermore, to better calculate similarity, they

used LOMO features and Hankel matrices to represent the appearance and motion features of targets, respectively.

### III. DATASET

#### A. Previous datasets

Existing MTMC tracking datasets with overlapping fields of view include: EPFL [48], CAMPUS [49], MvMHAT [43], WILDTRACK [50], and DIVOTrack [45]. Each of these datasets suffers from one or more issues, including limited scene diversity, uniform weather and lighting conditions, and unsatisfactory annotation quality. The scarcity of high-quality datasets limits the training and application of models in MTMC tracking. To address the limitations and enrich the diversity of existing datasets, we constructed a high-quality annotated dataset, named VisionTrack, which features complex lighting conditions and enhanced scene richness (shown in the right chart of Figure 4). A comparison with existing datasets is shown in Table I.

#### B. VisionTrack

1) *Data collection*: We captured video data using two drones, each equipped with a camera that has a resolution of 1920×1080. All videos were captured at a frame rate of 30 FPS, comprising approximately 116K frames and 1176K detection boxes. Both drones were moving during the recording process. To ensure dataset diversity, we selected different scenes with varying weather and lighting conditions, including sunny, overcast, dusk, night (shown in Figure 3). We also captured scenes with varying levels of crowd density, ranging from sparse large targets to dense small targets (shown in left chart of Figure 4). The dataset is split approximately 1:1, with half designated for training and the other half for testing. The videos from the two cameras were manually time-aligned. We also place a high emphasis on the protection of personal privacy within our dataset. All individuals appearing in the dataset have consented to the use of their images solely for scientific research purposes.

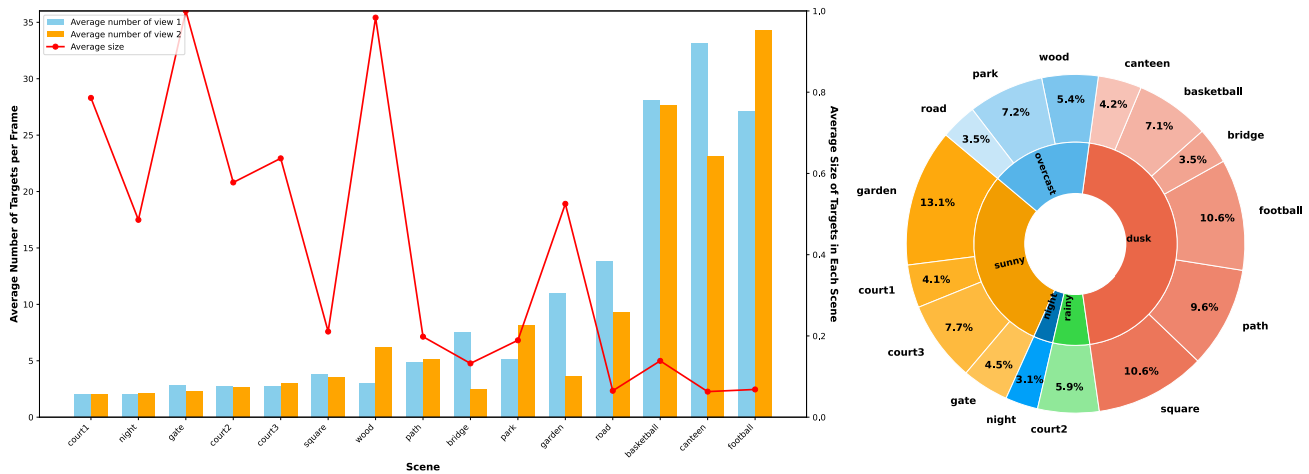


Fig. 4. Left chart: The red line graph represents the average size of each target in different scenes, while the bar chart represents the average number of targets per frame in different scenes. The VisionTrack dataset showcases various target densities in different scenes, ranging from densely packed small targets to sparsely distributed large targets. Right chart: The VisionTrack dataset covers a variety of weather and illumination conditions, including dark and low-light scenes.

TABLE I

COMPARISON BETWEEN MTMC TRACKING DATASETS WITH OVERLAPPING FIELDS OF VIEW. COMPARED TO EXISTING DATASETS, VISIONTRACK OFFERS ADVANTAGES IN TERMS OF THE NUMBER OF SCENES, QUANTITY OF IMAGES, COUNT OF TARGETS, COMPLEXITY OF LIGHTING CONDITIONS, AND THE NUMBER OF UAV VIEWS.

Dataset	Scenes	Views	Frames	Boxes	Moving camera	Low-light	UAV view
EPFL	5	3-4	97K	625K	×	×	×
CAMPUS	4	4	83K	490K	×	×	×
MvMHAT	1	3-4	31K	208K	✓	×	×
WILDTRACK	1	7	3K	40K	×	×	×
DIVOTrack	10	3	54K	560K	✓	×	one UAV
VisionTrack	<b>15</b>	2	<b>116K</b>	<b>1176K</b>	✓	✓	<b>two UAVs</b>

TABLE II  
NOTATION LIST OF GMT MODEL

$K$	The set of cameras in the scenario, $K = \{k_c\}_{c=1}^C$
$V$	The set of videos captured from the cameras, $V = \{v_c\}_{c=1}^C$
$M_c$	The set of all frames in video $v_c$ , $M_c = \{m_c^t\}_{t=1}^{T_c}$
$\Gamma_i$	The trajectory $\Gamma_i$ consisted of a bounding boxes set, $\Gamma_i = \{\tau_i^{ct}\}_{c=1, t=1}^{C, T}$
$\tau_i^{ct}$	The bounding box corresponding to $\Gamma_i$ in frame $m_c^t$
$P$	The set of detected targets, $P = \{p_n\}_{n=1}^N$
$p_n$	The target $p_n$ consisted of the bounding box position, time, and camera index, $p_n = (b_n, t_n, c_n)$
$f_n$	The fused feature of target $p_n$
$p_n \in \Gamma_i$	The detected target $p_n$ belongs to trajectory $\Gamma_i$
$p_i \leftrightarrow p_j$	The target $p_i$ and target $p_j$ belong to the same trajectory

2) *Annotation*: Our dataset annotation process was twofold. In the first step, annotators identified and assigned unique IDs to the same targets present in the overlapping fields of view from both cameras. In the second step, we employed the semi-automatic object tracking annotation software, Darklable, to annotate frame-by-frame the targets selected in the first step from the synchronized videos captured by the two cameras. This process was repeated until all targets in the videos were assigned unique IDs. Notably, for targets appearing in only one camera’s view, they were annotated solely within that view. We designed annotation guidelines for our MTMC tracking dataset, based on methods from multi-object tracking [51]:

- Even if a portion of the target is occluded, annotators are required to estimate the complete bounding box.
- When over half of the target’s body is out of the camera’s view, annotators disregard these targets.
- For any given target, a unique ID is maintained throughout the entire video sequence captured by both cameras.

#### IV. METHOD

To achieve robust, online MTMC tracking in overlapping fields of view, we introduce a novel transformer-based Global MTMC Tracking (GMT) model, as illustrated in Figure 2. Our GMT model consists of three main modules: a target detection module, a feature extraction and fusion module, and a global association module. These modules will be discussed in detail in the following three subsections. In subsection A, we present a brief definition of the MTMC tracking, as well as object detection module. Subsection B introduces a new method for target feature extraction and fusion in MTMC tracking. In subsection C, we propose an MTMC association module, comprising a global association transformer and a memory bank, capable of achieving online MTMC tracking and lost trajectory recovery.

##### A. Overview

1) *Problem definition*: Given a scenario with  $C$  cameras having overlapping fields of view, the cameras set is denoted

as  $K = \{k_c\}_{c=1}^C$ . The video stream  $v_c$  is captured from camera  $k_c$  and consists of  $T_c$  consecutive frames, represented as  $M_c = \{m_c^t\}_{t=1}^{T_c}$ , where  $m_c^t$  represents the frame at time  $t$  in the video stream  $v_c$ . The video streams captured from all cameras form the video stream set  $V = \{v_c\}_{c=1}^C$ . Our aim is to perform online detection and tracking of every target captured by the synchronized cameras. The goal is to assign IDs to the corresponding targets in different cameras and produce global trajectories. Assume there are  $I$  ground truth trajectories in the video stream set  $V$ , with each trajectory denoted by  $\Gamma_i$ , where  $\Gamma = \{\Gamma_i\}_{i=1}^I$ . A trajectory  $\Gamma_i$ , consisting of bounding boxes for the same target across all frames, is denoted by  $\Gamma_i = \{\tau_i^{ct}\}_{c=1, t=1}^{C, T}$ , where  $\tau_i^{ct}$  represents the bounding box of trajectory  $\Gamma_i$  in frame  $m_c^t$ .

$$\tau_i^{ct} = \begin{cases} (x_1^{ict}, y_1^{ict}, x_2^{ict}, y_2^{ict})^T & \text{if } \Gamma_i \text{ appears in } m_c^t \\ \emptyset & \text{otherwise} \end{cases} \quad (1)$$

2) *Object detection*: Given an image set  $M = \{m_c^t\}_{c=1, t=1}^{C, T}$  captured from  $C$  synchronized cameras over a time period  $T$ , the object detector processes each frame  $m_c^t$  and detects  $N_c^t$  targets. These detected targets in frame  $m_c^t$  are denoted as  $P^{ct} = \{p_n^{ct}\}_{n=1}^{N_c^t}$ .

The set of detected targets from all frames in image set  $M$  is denoted as  $P = \bigcup_{c=1}^C \bigcup_{t=1}^T P^{ct} = \{p_n\}_{n=1}^N$ , where  $N = \sum_{c=1}^C \sum_{t=1}^T N_c^t$ .

The corresponding bounding boxes for the detected targets in set  $P$  are represented as  $B = \{b_n\}_{n=1}^N$ , where  $b_n$  represents the spatial coordinates of the  $n^{\text{th}}$  detected target in set  $P$  and is given by  $b_n = (x_1^n, y_1^n, x_2^n, y_2^n)^T$ . Each detected target  $p_n$  is defined by its bounding box, temporal index  $t_n$ , and camera index  $c_n$ , where  $p_n = (b_n, t_n, c_n)$ .

Our pipeline's detection module can be integrated with most existing detectors for end-to-end training. We employ the CenterNet [25] with a DLA34 [52] backbone for object detection. CenterNet is an anchor-free detector based on key-point detection. Images are processed through the CenterNet to produce heatmaps, where peaks in the heatmaps correspond to object centers. The overall loss function for the network is defined as

$$\mathcal{L}_{\text{det}} = \mathcal{L}_k + \lambda_{\text{size}} \mathcal{L}_{\text{size}} + \lambda_{\text{off}} \mathcal{L}_{\text{off}} \quad (2)$$

where the keypoint loss  $\mathcal{L}_k$ , object size loss  $\mathcal{L}_{\text{size}}$ , and center offset loss  $\mathcal{L}_{\text{off}}$  are consistent with their definitions in the original paper [25]. The loss weights are set as  $\lambda_{\text{size}} = 0.1$  and  $\lambda_{\text{off}} = 1.0$ , which are also consistent with the original paper.

### B. Feature extraction module

Re-ID features are particularly effective in scenarios where targets have distinct appearances, enabling reliable identification across different camera views. However, relying solely on appearance features can be insufficient, especially in crowded scenes or when targets have similar visual characteristics. To address this limitation, our model also integrates spatio-temporal features. These features include the target's bounding box position, temporal information, and camera index. The

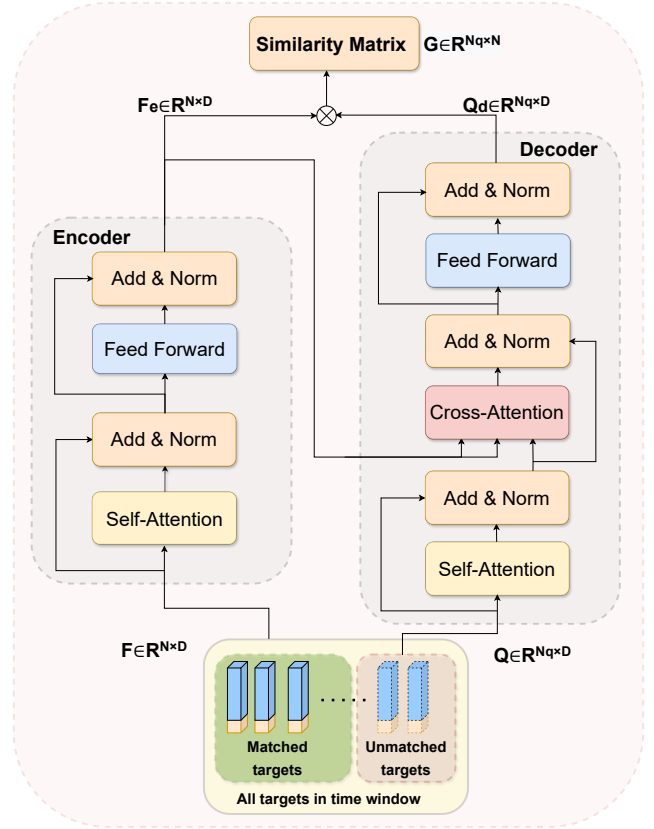


Fig. 5. Global association transformer: During online inference,  $Q$  represents the features of targets to be matched in the current frame, and  $F$  represents the features of all detected targets (including matched targets in historical frames and unmatched targets in the current frame) within the time window. During training,  $Q = F$ , where both the encoder and decoder inputs are the features of all detected targets.

bounding box position provides spatial context, indicating where the target is located within the frame. Temporal information captures the motion patterns of the target over time, and the camera index distinguishes between different camera views. We employ RoIAlign [53] to extract the Re-ID features of each detected target in the set  $P$ . These Re-ID features encapsulate the discriminative visual attributes of each detected target, aiding in distinguishing between different individuals even under challenging conditions such as occlusions or changes in viewpoint. The Re-ID feature for the detected target  $p_n$  is denoted as  $f_n^{\text{roi}}$ . The Re-ID features for all detected targets in  $P$  are concatenated as  $F^{\text{roi}} = \text{concat}(\{f_n^{\text{roi}}\}_{n=1}^N)$ , where  $N$  is the number of targets. Additionally, we merge the box position, temporal, and camera index features of each detected target to form a comprehensive spatio-temporal feature vector. This feature incorporates spatial location information, temporal dynamics, and camera-specific attributes, thereby enriching the feature representation with contextual information essential for accurate target association across camera views. The box position, temporal, and camera index features of the detected target  $p_n$  are merged to form the spatio-temporal feature vector:  $f_n^{\text{st}} = \left( \frac{x_1^n}{w}, \frac{y_1^n}{h}, \frac{x_2^n}{w}, \frac{y_2^n}{h}, \frac{t_n}{T}, \frac{c_n}{C} \right)$ , where  $w$  and  $h$  are the width and height of the frame containing  $p_n$ . The

spatio-temporal features for all targets in  $P$  are concatenated as  $F^{\text{st}} = \text{concat}(\{f_n^{\text{st}}\}_{n=1}^N)$ . By passing  $f_n^{\text{roi}}$  and  $f_n^{\text{st}}$  through Re-ID feature encoder  $H_{\text{roi}}$  and spatio-temporal feature encoder  $H_{\text{st}}$ , respectively, the fused feature for target  $p_n$  is constructed as  $f_n = \text{concat}(H_{\text{roi}}(f_n^{\text{roi}}), H_{\text{st}}(f_n^{\text{st}})) \in \mathbb{R}^D$ , where  $H_{\text{roi}}(f_n^{\text{roi}}) \in \mathbb{R}^{D_{\text{roi}}}$  and  $H_{\text{st}}(f_n^{\text{st}}) \in \mathbb{R}^{D_{\text{st}}}$ . Here,  $D$  is the dimension of the fused feature  $f_n$ ,  $D_{\text{roi}}$  is the dimension of the output Re-ID feature, and  $D_{\text{st}}$  is the dimension of the output spatio-temporal feature, with  $D = D_{\text{st}} + D_{\text{roi}}$ . The fused features of targets in  $P$ , denoted as  $F = \text{concat}(\{f_n\}_{n=1}^N) \in \mathbb{R}^{N \times D}$ , serve as inputs for the global association module. Overall, the fusion of these diverse features results in a more robust and comprehensive representation of each target. By combining appearance and spatio-temporal information, our model can better handle challenging scenarios where targets may look similar but move differently or when their appearance changes due to varying environmental conditions across cameras.

### C. Global association module

In Section B, we acquired the fused features  $F$  of all detected targets within the image set  $M$ . The global association module (shown in Figure 5) enhances and interrelates target features, producing a similarity matrix between targets to be matched in the current frame and detected targets in the time window (including matched targets in the historical frames and unmatched targets in the current frame). This matrix is then used with the Hungarian algorithm to establish relationships between unmatched targets and matched targets and to produce global trajectories. For targets that fail to match trajectories, they will be associated with historical trajectories stored in the memory bank to determine whether new trajectories should be generated.

1) *Targets association learning*: Our global association transformer is constructed with an encoder and a decoder layer. The encoder processes  $F \in \mathbb{R}^{N \times D}$ , representing the features of all detected targets within a time window, where  $N$  is the number of all detected targets. The decoder processes  $Q \in \mathbb{R}^{N_q \times D}$ , representing the features of unmatched targets, where  $N_q$  is the number of unmatched targets. This architecture is designed to explore the associations between unmatched targets and matched targets, thereby facilitating the identification and tracking. The encoder utilizes self-attention layer and feed-forward layer to enhance the features  $F$ . The enhanced features output from the encoder are denoted as  $F_e \in \mathbb{R}^{N \times D}$ . In the decoder layer, cross-attention operations are conducted between  $F_e$  and the features output from the decoder's self-attention layer. The enhanced features output by the decoder are  $Q_d \in \mathbb{R}^{N_q \times D}$ . The similarity matrix between  $Q$  and  $F$  is obtained by the matrix multiplication  $G = Q_d F_e^T \in \mathbb{R}^{N_q \times N}$ . Here,  $G_{ij}$  is an element of the matrix  $G$  and represents the score indicating the likelihood that the  $i^{\text{th}}$  target in  $Q$  and the  $j^{\text{th}}$  target in  $F$  belong to the same trajectory.

To determine the correlation between each detected target and the ground truth trajectory, we follow an assignment method consistent with object detection. If the ground truth bounding box  $\tau_k^{c_n t_n}$  from trajectory  $\Gamma_k$  in frame  $m_{c_n}^{t_n}$  has the

highest IoU with bounding box  $b_n$  (corresponding to target  $p_n$ ) among all targets detected in  $m_{c_n}^{t_n}$  and this IoU exceeds 0.6, we determine that target  $p_n$  belongs to trajectory  $\Gamma_k$ . Otherwise,  $p_n$  has no association with  $\Gamma_k$ .

$$p_n \begin{cases} \in \Gamma_k & \text{if } \arg \max_i \text{IoU}(\tau_k^{c_n t_n}, b_i) = n \\ & \text{and } \text{IoU}(\tau_k^{c_n t_n}, b_n) > 0.6 \\ \notin \Gamma_k & \text{otherwise} \end{cases} \quad (3)$$

During network training, the trajectory to which each target belongs is known. Therefore, the features of all targets are used as inputs for both the encoder and the decoder, i.e.,  $Q = F$  and  $G \in \mathbb{R}^{N \times N}$ , where the features of all targets function as queries to establish associations between any two targets. This configuration enables the model to effectively learn the relationships and associations among targets, both within the same trajectory and across different trajectories during the training stage.

We represent the case where  $p_i$  and  $p_j$  belong to the same trajectory as  $p_i \leftrightarrow p_j$ .  $G_{ij}$  represents the similarity score of  $p_i \leftrightarrow p_j$ . Considering that  $p_i$  in frame  $m_c^t$  may not correspond to any target, we define the similarity score of  $p_i \leftrightarrow \emptyset$  as  $g_{i0} = 0$ . We apply softmax to the similarity matrix  $G$  separately for each frame to obtain the association matrix  $H$ . For the frame  $m_{c_j}^{t_j}$  where the target  $p_j$  is detected, the element  $H_{ij}$  denotes the probability distribution of  $p_i \leftrightarrow p_j$ . This is achieved by normalizing the similarity scores  $G_{ij}$  across all potential targets within the same frame  $m_{c_j}^{t_j}$ , ensuring that the sum of probabilities for  $p_i$  associating with any target (including the possibility that  $p_i$  does not correspond to any target, i.e.,  $p_i \leftrightarrow \emptyset$ ) in that frame equals 1.

$$H_{ij} = \frac{e^{G_{ij}}}{e^{g_{i0}} + \sum_{q=1}^N \mathbf{1}_{(t_q=t_j \text{ and } c_q=c_j)} e^{G_{iq}}} \quad (4)$$

where  $(t_q = t_j \text{ and } c_q = c_j)$  denotes target  $p_q$  is detected in frame  $m_{c_j}^{t_j}$  and  $\mathbf{1}_{(f)}$  is  $\begin{cases} 1 & \text{if } f = \text{true} \\ 0 & \text{if } f = \text{false} \end{cases}$ .

Similarly, on image  $m_c^t$ , the probability distribution  $p_i \leftrightarrow \emptyset$  is

$$h_{i0}^{ct} = \frac{e^{g_{i0}}}{e^{g_{i0}} + \sum_{q=1}^N \mathbf{1}_{(t_q=t \text{ and } c_q=c)} e^{G_{iq}}} \quad (5)$$

where  $(t_q = t \text{ and } c_q = c)$  denotes target  $p_q$  is in frame  $m_c^t$ .

The ground truth of the association matrix  $H$  is represented by  $X$ .  $X_{ij} = 1$  indicates  $p_i \leftrightarrow p_j$ .

$$X_{ij} = \begin{cases} 1 & \text{if } p_i \leftrightarrow p_j \\ 0 & \text{otherwise} \end{cases} \quad (6)$$

Similarly, the ground truth for  $h_{i0}^{ct}$  is denoted as  $x_{i0}^{ct}$ .  $x_{i0}^{ct} = 1$  indicates  $p_i \leftrightarrow \emptyset$  in frame  $m_c^t$ .

$$x_{i0}^{ct} = \begin{cases} 1 & \text{if } p_i \leftrightarrow \emptyset \text{ in } m_c^t \\ 0 & \text{otherwise} \end{cases} \quad (7)$$

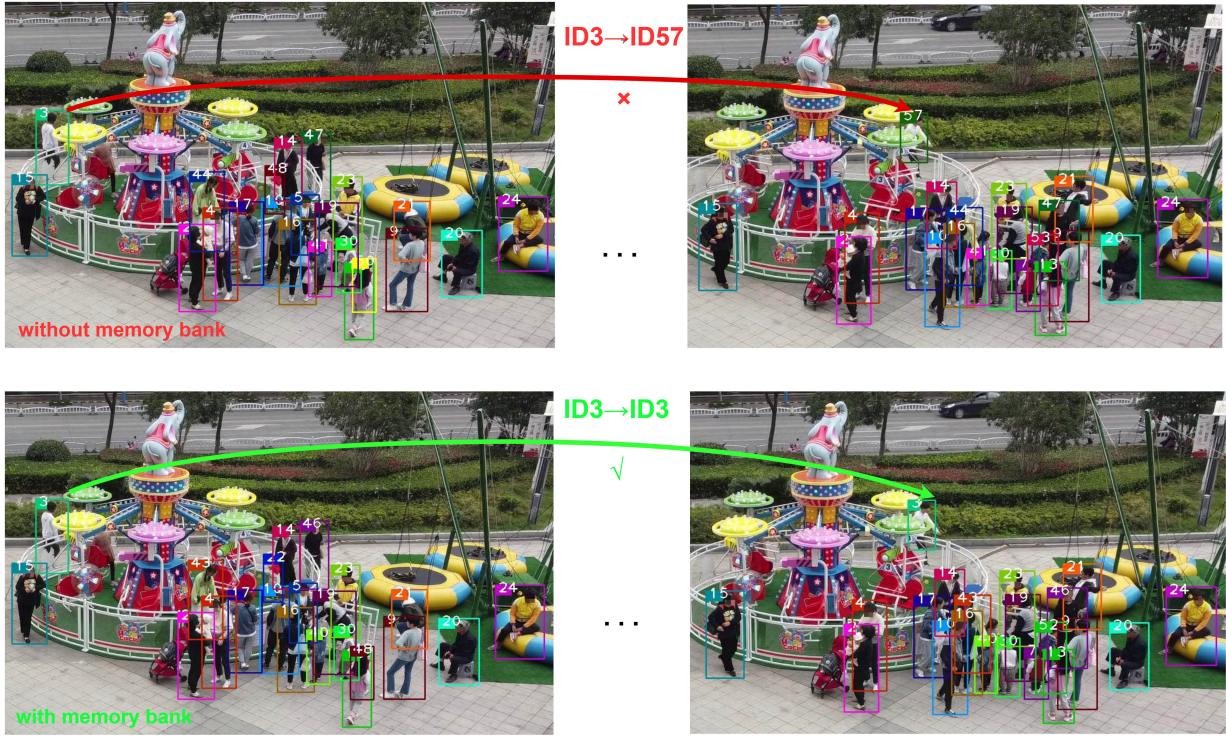


Fig. 6. Comparison of tracking performance with and without the memory bank module. The target wearing white clothing experienced continuous occlusion from the left image until reappearing in the right image, spanning a duration of 152 frames, which exceeds the time window limit. The absence of such a module could lead to ID switching errors.

Given that each target has a unique corresponding target in every frame, we use the multi-object classification cross-entropy loss in each frame to calculate the association loss between targets. In frame  $m_c^t$ , the loss is calculated by:

$$\mathcal{L}_{asso}^{ct} = -\frac{1}{N} \left( \sum_{i=1}^N \left( \sum_{j=1}^N X_{ij} \log(H_{ij}) \cdot 1_{(t_j=t \text{ and } c_j=c)} + x_{i0}^{ct} \log(h_{i0}^{ct}) \right) \right) \quad (8)$$

We take the sum of cross-entropy losses on all frames as the total target association loss:

$$\mathcal{L}_{asso} = \sum_{c=1}^C \sum_{t=1}^T \mathcal{L}_{asso}^{ct} \quad (9)$$

The complete network is optimized through the following loss function:

$$\mathcal{L} = \mathcal{L}_{det} + \mathcal{L}_{asso} \quad (10)$$

2) *Online Interference*: During online inference, we process the video stream using a sliding time window with a size of  $W$  and a step size of  $S = 1$ . At time  $t$ , from the image set  $\{m_c^t\}_{c=1}^C$  obtained from all camera views, we detect  $N_t$  targets, denoted as  $P^t = \{p_n^t\}_{n=1}^{N_t}$ , with their corresponding fused features given by  $F^t = \{f_n^t\}_{n=1}^{N_t}$ . Let  $T$  represent the current time point. The starting time of the window is then calculated by  $T_s = \max(1, T - W + 1)$ . We maintain a historical cache for all  $N$  targets within the time window, encompassing the fused features of all targets,

where  $N = \sum_{t=T_s}^T N_t$ . All targets in time window are denoted as  $P = \bigcup_{t=T_s}^T P^t = \{p_n\}_{n=1}^N$ . The input  $F$  for the encoder of global association module represents features of all targets in time window, where  $F = \text{concat}(\{F^t\}_{t=T_s}^T)$  and  $F \in \mathbb{R}^{N \times D}$ . The input  $Q$  for the decoder of global association module represents the features of the unmatched targets in the current frame, where  $Q = \text{concat}(F^T)$  and  $Q \in \mathbb{R}^{N_T \times D}$ . The global association transformer produces a similarity matrix  $G \in \mathbb{R}^{N_T \times N}$ , indicating the similarity scores between each unmatched target in the current frame and all targets in the time window. Assuming there are  $N_R$  trajectories corresponding to the matched targets within the current time window, denoted as  $\Gamma = \{\Gamma_i\}_{i=1}^{N_R}$ . As the targets within the time window, except for those in the current frame, have already been assigned trajectories in previous inference steps, we transform the similarity matrix  $G$  into  $G'$ , representing associations between unmatched targets and existing trajectories, where  $G' \in \mathbb{R}^{N_T \times N_R}$ .

$$G' = GM$$

where the element  $M_{ij}$  in the matrix  $M$  represents the correspondence between target  $p_i$  in  $P$  and trajectory  $\Gamma_j$  in  $\Gamma$ ,  $M_{ij} = \begin{cases} 1 & \text{if } p_i \in \Gamma_j \\ 0 & \text{if } p_i \notin \Gamma_j \end{cases}$  and  $M \in \mathbb{R}^{N \times N_R}$

We use the Hungarian algorithm to  $G'$  to match the current frame's targets with all trajectories within the time window. We set the threshold for successfully associating unmatched targets with matched trajectories to  $\theta_1$ . If the association score exceeds the threshold  $\theta_1$ , the target is associated with the corresponding trajectory, forming a global trajectory. Targets

TABLE III

COMPARISON OF MTMC TRACKING RESULTS ON THE EPFL, CAMPUS, MvMHAT, WILDTRACK, DIVOTRACK AND VISIONTRACK DATASET. CA AND C1 RESPECTIVELY STAND FOR CVMA AND CVIDF1. THE BEST TWO RESULTS ARE SHOWN IN RED AND BLUE.

Methods	EPFL		CAMPUS		MvMHAT		WILDTRACK		DIVOTrack		VisionTrack	
	CA↑	C1↑	CA↑	C1↑	CA↑	C1↑	CA↑	C1↑	CA↑	C1↑	CA↑	C1↑
OSNet	73.0	40.3	58.8	47.8	92.6	87.7	10.8	18.2	33.0	44.9	63.8	64.4
Strong	75.6	45.2	63.4	55.0	49.0	55.1	28.6	41.6	39.1	44.7	16.9	43.0
AGW	73.9	43.2	60.8	52.8	92.5	86.6	15.6	23.8	54.3	55.3	70.1	68.4
MvMHAT	30.5	33.7	56.0	55.6	70.1	68.4	10.3	16.2	58.2	60.7	39.2	53.6
CrossMOT	74.4	47.3	65.6	61.2	92.3	87.4	42.3	56.7	68.8	69.1	64.5	64.4
<b>GMT</b>	76.1	71.2	71.0	77.6	96.5	97.0	61.0	60.0	75.3	78.6	76.0	81.4

TABLE IV

COMPARISON OF MTMC TRACKING RESULTS ON EACH SCENE OF VISIONTRACK DATASET. CA AND C1 RESPECTIVELY STAND FOR CVMA AND CVIDF1. THE BEST TWO RESULTS ARE SHOWN IN RED AND BLUE.

Scenes	Garden		Night		Gate		Square		Path	
	CA↑	C1↑	CA↑	C1↑	CA↑	C1↑	CA↑	C1↑	CA↑	C1↑
OSNet	68.1	68.7	69.2	63.2	86.9	90.8	85.6	80.6	57.4	44.9
Strong	42.5	56.6	3.3	34.2	6.1	42.4	9.1	47.5	13.9	49.7
AGW	76.5	73.8	66.2	61.0	86.4	90.4	87.1	87.8	70.2	78.0
MvMHAT	75.2	72.1	62.1	61.5	86.7	82.2	86.3	85.3	45.3	62.4
CrossMOT	62.1	67.9	74.8	52.6	80.4	78.2	83.2	91.0	62.2	64.7
<b>GMT</b>	82.3	81.5	48.6	73.4	85.9	91.2	87.2	90.4	77.6	86.4

Scenes	Football		Woods		Park		Road		Bridge	
	CA↑	C1↑	CA↑	C1↑	CA↑	C1↑	CA↑	C1↑	CA↑	C1↑
OSNet	78.8	74.5	75.9	53.5	43.8	59.1	-18.5	37.6	2.0	20.4
Strong	21.0	47.3	14.9	30.8	10.2	37.3	-37.3	25.4	-0.2	18.1
AGW	81.6	78.0	74.9	61.3	63.1	63.3	-4.8	42.7	2.4	19.4
MvMHAT	32.1	53.6	67.0	59.0	20.8	45.4	-28.5	29.5	-0.3	19.2
CrossMOT	75.5	71.7	36.7	50.9	49.6	58.5	-5.8	39.8	-0.9	19.1
<b>GMT</b>	83.5	86.1	79.0	83.5	74.5	83.3	11.2	52.8	20.7	45.1

Scenes	Basketball		Canteen		Court1		Court2		Court3	
	CA↑	C1↑	CA↑	C1↑	CA↑	C1↑	CA↑	C1↑	CA↑	C1↑
OSNet	76.5	57.3	28.7	54.1	95.2	75.8	86.0	89.9	77.9	84.8
Strong	7.0	33.2	29.3	46.8	2.5	38.7	-11.7	44.9	1.2	44.4
AGW	84.3	64.5	33.9	55.2	93.2	74.8	85.4	91.9	98.0	88.2
MvMHAT	48.3	48.3	28.0	50.8	93.1	76.5	84.6	88.8	96.2	87.8
CrossMOT	72.1	59.9	47.4	54.9	87.4	83.3	83.1	90.9	96.2	97.5
<b>GMT</b>	86.6	86.9	59.8	71.8	97.3	98.6	93.6	96.9	92.5	96.2

with association scores below the threshold  $\theta_1$  are added to the buffer  $\{f_n^u\}_{n=1}^{N_u}$ , where  $f_n^u$  is the fused feature of the unmatched targets and  $N_u$  is the number of unmatched targets.

Due to the limitation of the time window size, we cannot recover trajectories appearing outside the time window. We maintain a memory bank to store features of trajectories that appeared but have been absent for more than  $W$  frames. Assuming the memory bank retains  $R$  trajectories, the memory bank is represented by  $\{\tilde{f}^r\}_{r=1}^R$ . For trajectory  $r$ , the average feature of its last  $N_{mem}$  appearances represents the trajectory's feature in the memory bank:  $\tilde{f}^r = \frac{1}{N_{mem}} \sum_{n=1}^{N_{mem}} f_n^r$ , where  $f_n^r$  is the fused feature of the target that belongs to trajectory  $r$ . We use global association transformer to calculate association matrix between unmatched targets and historical trajectories, where the features passed to the global association transformer are  $F = \text{concat}(\{\tilde{f}^r\}_{r=1}^R)$  and  $Q = \text{concat}(\{f_n^u\}_{n=1}^{N_u})$ . We set the threshold for successfully matching unmatched targets

with trajectories in the memory bank to  $\theta_2$ . For targets with association scores above  $\theta_2$ , they are associated with historical trajectories. Targets with scores below the threshold  $\theta_2$  will initiate the generation of a new trajectory.

## V. EXPERIMENTS

### A. Implementation details

1) *Training*: We employ DLA-34 [54] and CenterNet [25] as the backbone and object detector respectively. For the VisionTrack dataset, original images are first resized proportionally to  $1280 \times 720$ . Each image side is then scaled by a random factor between 0.8 and 1.2 before being fed into the backbone. We utilized the Adam optimizer with an initial learning rate of  $10^{-4}$  to pretrain the backbone and object detector on the CrowdHuman [55] dataset for 45,000 iterations, with a batch size of 32. Subsequently, we integrated the full network and co-trained global association transformer



TABLE V  
COMPARISON OF SINGLE-CAMERA TRACKING METRICS ON VISIONTRACK DATASET. THE BEST TWO RESULTS ARE SHOWN IN RED AND BLUE.

	MOTA $\uparrow$	MOTP $\uparrow$	IDF1 $\uparrow$	MT $\uparrow$	ML $\downarrow$	HOTA $\uparrow$	DetA $\uparrow$	AssA $\uparrow$	FPL	FN $\downarrow$	IDS $\downarrow$
OSNet	77.4	80.3	68.4	79.8	5.1	57.8	62.8	53.7	174982	187397	1973
Strong	19.1	78.7	45.7	50.4	30.3	41.3	34.1	50.4	304574	317473	2698
AGW	77.0	80.3	77.0	79.5	5.4	59.5	62.9	57.0	160693	174219	2243
MvMHAT	76.9	80.4	66.0	79.5	5.1	56.3	62.5	51.3	189075	200258	1680
CrossMOT	75.6	78.5	65.8	76.0	5.7	54.5	60.8	49.3	189582	201867	1767
GMT	79.7	81.2	82.7	76.9	7.7	67.0	65.0	69.5	78481	115016	843

with the object detector on the VisionTrack datasets for 18,000 iterations using Adam, starting with a learning rate of  $5 \times 10^{-5}$  and a batch size of 18. Training was conducted on two NVIDIA A6000 48G GPUs.

2) *Inference*: For the VisionTrack, we set the object detection threshold at 0.52. In the feature extraction module, the dimensions of appearance features and spatio-temporal features are set as  $D_{\text{roi}} = 1024$  and  $D_{\text{st}} = 128$  respectively. In the global association module, thresholds for associating existing trajectories and reviving historical ones are set as  $\theta_1 = 0.1$  and  $\theta_2 = 0.2$  respectively. During testing, we set the time window size  $W = 60$ , and the memory bank stores the average features of the last  $N_{\text{mem}} = 10$  appearances of the targets. For model output, trajectories shorter than 10 frames are discarded to reduce false positives from object detection. Inference was conducted on one NVIDIA TITAN RTX 24G GPU.

### B. Evaluation Metrics

Differing from single-camera tracking, multi-camera tracking metrics should be able to evaluate the Re-ID of the same target across different cameras. Hence, we adopt the cross-view IDF1 (CVIDF1) metric and the cross-view matching accuracy (CVMA) metric proposed in [56] as our evaluation metrics. CVIDF1, an ID-based metric, originates from the IDF1 metric in single-camera tracking and is defined as:

$$CVIDF1 = \frac{2 \times CVIDP \times CVIDR}{CVIDP + CVIDR} \quad (11)$$

where CVIDP and CVIDR denote the inter-camera tracking precision and recall, respectively. CVMA, which assesses multi-target tracking accuracy, originates from the MOTA metric from single-camera tracking and is defined as:

$$CVMA = 1 - \left( \frac{\sum_t m_t + \text{fp}_t + 2\text{mme}_t}{\sum_t g_t} \right) \quad (12)$$

where  $m_t$ ,  $\text{fp}_t$ , and  $\text{mme}_t$  represent missed detections, false positives, and inter-camera mismatches, respectively.  $g_t$  indicates the total number of detected targets across all cameras.

### C. Comparison with Other SOTA Methods

To evaluate the performance of our model, we conducted experiments on six MTMC tracking datasets with overlapping fields of view: EPFL [48], CAMPUS [49], MvMHAT [43], WILDTRACK [50], DIVOTrack [45], and VisionTrack. We compared our model against existing methods: OSNet [57], Strong [58], AGW [59], MvMHAT [43], and CrossMOT [45]. Table III shows that our model substantially outperforms existing approaches across all datasets. On the VisionTrack

dataset, our model achieved a performance of 76.0 CVMA (CA) and 81.4 CVIDF1 (C1), outperforming the second-best model by 5.9 in CA and 13.0 in C1. Tracking results on each scene of VisionTrack are shown in Table IV. We achieved the best and second-best results in the vast majority of scenes. We also compared our model with the other models on the single-camera tracking metrics, as shown in Table V. Our model achieves a 79.7 MOTA, 82.7 IDF1, and 67.0 HOTA. This is also better than the other models.

### D. Ablation studies

To validate each module within our model, we conducted ablation studies on the feature extraction module, global association module, and memory bank module using the VisionTrack dataset. To prevent any bias from the object detector's performance influencing the tracking results, the same object detection results were used during testing.

1) *Feature extraction module*: To further investigate the impact of integrating spatio-temporal features into the Re-ID features for inter-camera target association, we present our ablation study results in Table VI. Under the condition of maintaining a constant Re-ID feature dimension  $D_{\text{roi}} = 1024$ , we varied the dimension of the spatio-temporal feature  $D_{\text{st}}$ . Optimal metrics for CA and C1 are observed when  $D_{\text{st}}$  is set to 128 and 64, respectively. In comparison to the model without spatio-temporal feature, there is an enhancement of 0.4 and 0.3 in the CVMA and CVIDF1 metrics, respectively. On the DIVOTrack dataset, we observed enhancements of 1.4 in CVMA and 1.3 in CVIDF1 upon integrating spatio-temporal features into our model. The less gains on the VisionTrack dataset are largely attributable to the frequent camera movements during our dataset collection, which diminished the impact of spatio-temporal features. Based on our experimental results, we can state that integrating an appropriate proportion of spatio-temporal features into the Re-ID features enhances target associations. However, if the proportion of the spatio-temporal feature becomes overly dominant in the fused feature, the tracking performance degrades.

2) *Global association module*: We demonstrate the impact of varying the number of heads in global association transformer on tracking performance in Table VI. We observe that the number of heads significantly affects the model's performance, necessitating the determination of the optimal number of heads through prior experimentation. Table VI illustrates the impact of varying the number of attention layers on tracking results. Results indicate that increasing the number of attention layers does not enhance model performance. Consequently, we adopted a default structure for our model,

TABLE VI  
ABLATION STUDIES ON VARIOUS PARAMETERS. THE NUMBER IN BOLD REPRESENTS THE BEST RESULT.

Parameter	$D_{st}$	CA $\uparrow$	C1 $\uparrow$	Parameter	$W$	CA $\uparrow$	C1 $\uparrow$
Feature Dimension	0	75.6	81.2	Window Size	30	75.7	80.3
	64	75.7	<b>81.5</b>		45	75.7	81.4
	128	<b>76.0</b>	81.4		60	<b>76.0</b>	81.4
	256	75.9	81.0		75	75.4	<b>81.8</b>
	512	74.5	80.5		90	75.0	81.5
Parameter	$H$	CA $\uparrow$	C1 $\uparrow$	Parameter	$N_{enc} : N_{dec}$	CA $\uparrow$	C1 $\uparrow$
Number of Heads	1	73.4	80.4	Attention Layers	1:1	<b>76.0</b>	<b>81.4</b>
	4	74.1	80.3		2:1	74.8	80.3
	8	<b>76.0</b>	<b>81.4</b>		1:2	75.5	80.9
	16	74.2	81.3		2:2	75.8	81.1
	32	75.2	81.4		3:3	75.6	80.7

TABLE VII  
COMPARISON OF MTMC TRACKING RESULTS ON EACH SCENE OF VISIONTRACK DATASET. THE NUMBER IN BOLD REPRESENTS THE BEST RESULT. CA AND C1 RESPECTIVELY STAND FOR CVMA AND CVIDF1.

	backbone	CenterNet	Re-ID Encoder	ST Encoder	Transformer
Flops	183.8G	43.3G	0.2G	0.8M	0.1G
Params	15.2M	0.7M	9.1M	0.03M	5M

which consists of an encoder layer and a decoder layer, each equipped with 8 heads.

3) *Memory bank module*: As illustrated in Figure 6, the integration of the memory bank module enables the model to recover lost trajectories. Without the memory bank module, a pedestrian dressed in white who re-emerges after a prolonged occlusion (lasting 152 frames, which surpasses the size of the temporal window  $W$ ) is mistakenly recognized as a new target, with the ID switching from ID3 to ID57. However, with the memory bank module, when the target reappears, it successfully matches with the historical trajectory with ID3 in the memory bank.

4) *Hyperparameters*: To further investigate the impact of hyperparameter settings on model performance, we examine the effects of using various temporal window sizes during inference. The experimental results are presented in Table VI. We observe that modestly increasing the size of the temporal window aids in enhancing tracking performance. However, an excessively large temporal window inversely affects performance, potentially due to the increased complexity in associating targets with more distant temporal information. To balance inference speed and model performance, we select a temporal window size of  $W = 60$  as our default hyperparameter.

5) *Model parameter size and real-time performance*: Inference was conducted on one NVIDIA TITAN RTX 24G GPU. The GMT model achieves an average frame rate of 7.5 fps across various scenes. As shown in Table VII, the runtime of the backbone occupies a large proportion in the network. Future work could explore the use of more lightweight networks to further enhance real-time performance.

## VI. CONCLUSION

We propose a transformer-based global MTMC tracking model, GMT. The GMT model globally associates all targets

appearing in different camera within a time window, generating global trajectories from detections at once. To enhance the feature representation of the targets, we integrate spatial-temporal features with the target Re-ID features, enabling the target features to simultaneously capture appearance and motion patterns. To recover lost trajectories, we incorporate a memory bank module to preserve features of historical trajectories. In addressing the issues of insufficient diversity of scenes, lack of low-light environments, and unsatisfactory annotation quality in existing datasets, we have developed a new large-scale MTMC tracking dataset, VisionTrack. GMT model exhibits superior performance across multiple datasets in diverse scenes and lighting conditions, demonstrating its robustness.

Our model employs a simple network to extract target Re-ID features. For some severely occluded targets, the model fails to accurately associate them. Future research could focus on designing a more powerful Re-ID encoder specifically tailored for MTMC tracking.

## REFERENCES

- [1] P. Li, J. Zhang, Z. Zhu, Y. Li, L. Jiang, and G. Huang, "State-aware re-identification feature for multi-target multi-camera tracking," in *Proceedings of the IEEE/CVF Conference on Computer Vision and Pattern Recognition Workshops*, 2019, pp. 0–0.
- [2] F. Yang, H. Lu, and M.-H. Yang, "Robust superpixel tracking," *IEEE Transactions on Image Processing*, vol. 23, no. 4, pp. 1639–1651, 2014.
- [3] J. Fan, X. Shen, and Y. Wu, "What are we tracking: A unified approach of tracking and recognition," *IEEE transactions on image processing*, vol. 22, no. 2, pp. 549–560, 2012.
- [4] D. Li, X. Wei, X. Hong, and Y. Gong, "Infrared-visible cross-modal person re-identification with an x modality," in *Proceedings of the AAAI conference on artificial intelligence*, vol. 34, no. 04, 2020, pp. 4610–4617.
- [5] S. Yogamani, C. Hughes, J. Horgan, G. Sistu, P. Varley, D. O’Dea, M. Uricar, S. Milz, M. Simon, K. Amende *et al.*, "Woodscape: A multi-task, multi-camera fisheye dataset for autonomous driving," in *Proceedings of the IEEE/CVF International Conference on Computer Vision*, 2019, pp. 9308–9318.
- [6] S. Panev and A. Manolova, "Improved multi-camera 3d eye tracking for human-computer interface," in *2015 IEEE 8th International Conference on Intelligent Data Acquisition and Advanced Computing Systems: Technology and Applications (IDAACS)*, vol. 1. IEEE, 2015, pp. 276–281.
- [7] C. d. Leo and B. S. Manjunath, "Multicamera video summarization and anomaly detection from activity motifs," *ACM Transactions on Sensor Networks (TOSN)*, vol. 10, no. 2, pp. 1–30, 2014.

- [8] Z. Ma, X. Wei, X. Hong, and Y. Gong, "Bayesian loss for crowd count estimation with point supervision," in *Proceedings of the IEEE/CVF international conference on computer vision*, 2019, pp. 6142–6151.
- [9] J. Ferryman and A. Shahrokni, "Pets2009: Dataset and challenge," in *2009 Twelfth IEEE international workshop on performance evaluation of tracking and surveillance*. IEEE, 2009, pp. 1–6.
- [10] Z. Tang, M. Naphade, M.-Y. Liu, X. Yang, S. Birchfield, S. Wang, R. Kumar, D. Anastasiu, and J.-N. Hwang, "Cityflow: A city-scale benchmark for multi-target multi-camera vehicle tracking and re-identification," in *Proceedings of the IEEE/CVF Conference on Computer Vision and Pattern Recognition*, 2019, pp. 8797–8806.
- [11] Y. Xu, X. Liu, L. Qin, and S.-C. Zhu, "Cross-view people tracking by scene-centered spatio-temporal parsing," in *Proceedings of the AAAI conference on artificial intelligence*, vol. 31, no. 1, 2017.
- [12] M. Hofmann, D. Wolf, and G. Rigoll, "Hypergraphs for joint multi-view reconstruction and multi-object tracking," in *Proceedings of the IEEE Conference on Computer Vision and Pattern Recognition*, 2013, pp. 3650–3657.
- [13] E. Ristani and C. Tomasi, "Features for multi-target multi-camera tracking and re-identification," in *Proceedings of the IEEE conference on computer vision and pattern recognition*, 2018, pp. 6036–6046.
- [14] O. Javed, K. Shafique, Z. Rasheed, and M. Shah, "Modeling inter-camera space-time and appearance relationships for tracking across non-overlapping views," *Computer Vision and Image Understanding*, vol. 109, no. 2, pp. 146–162, 2008.
- [15] N. Wojke, A. Bewley, and D. Paulus, "Simple online and realtime tracking with a deep association metric," in *2017 IEEE international conference on image processing (ICIP)*. IEEE, 2017, pp. 3645–3649.
- [16] Y. Zhang, C. Wang, X. Wang, W. Zeng, and W. Liu, "Fairmot: On the fairness of detection and re-identification in multiple object tracking," *International Journal of Computer Vision*, vol. 129, pp. 3069–3087, 2021.
- [17] N. Jiang, S. Bai, Y. Xu, C. Xing, Z. Zhou, and W. Wu, "Online inter-camera trajectory association exploiting person re-identification and camera topology," in *Proceedings of the 26th ACM international conference on Multimedia*, 2018, pp. 1457–1465.
- [18] T. I. Amosa, P. Sebastian, L. I. Izhar, O. Ibrahim, L. S. Ayinla, A. A. Bahashwan, A. Bala, and Y. A. Samaila, "Multi-camera multi-object tracking: A review of current trends and future advances," *Neurocomputing*, vol. 552, p. 126558, 2023.
- [19] W. Chen, L. Cao, X. Chen, and K. Huang, "An equalized global graph model-based approach for multicamera object tracking," *IEEE Transactions on Circuits and Systems for Video Technology*, vol. 27, no. 11, pp. 2367–2381, 2016.
- [20] W. Liu, O. Camps, and M. Sznajder, "Multi-camera multi-object tracking," *arXiv preprint arXiv:1709.07065*, 2017.
- [21] S. Ren, K. He, R. Girshick, and J. Sun, "Faster r-cnn: Towards real-time object detection with region proposal networks," *Advances in neural information processing systems*, vol. 28, 2015.
- [22] W. Liu, D. Anguelov, D. Erhan, C. Szegedy, S. Reed, C.-Y. Fu, and A. C. Berg, "Ssd: Single shot multibox detector," in *Computer Vision—ECCV 2016: 14th European Conference, Amsterdam, The Netherlands, October 11–14, 2016, Proceedings, Part I 14*. Springer, 2016, pp. 21–37.
- [23] J. Redmon and A. Farhadi, "Yolo9000: better, faster, stronger," in *Proceedings of the IEEE conference on computer vision and pattern recognition*, 2017, pp. 7263–7271.
- [24] J. Redmon, S. Divvala, R. Girshick, and A. Farhadi, "You only look once: Unified, real-time object detection," in *Proceedings of the IEEE conference on computer vision and pattern recognition*, 2016, pp. 779–788.
- [25] X. Zhou, D. Wang, and P. Krähenbühl, "Objects as points," *arXiv preprint arXiv:1904.07850*, 2019.
- [26] N. Carion, F. Massa, G. Synnaeve, N. Usunier, A. Kirillov, and S. Zagoruyko, "End-to-end object detection with transformers," in *European conference on computer vision*. Springer, 2020, pp. 213–229.
- [27] C. Fu, K. Lu, G. Zheng, J. Ye, Z. Cao, B. Li, and G. Lu, "Siamese object tracking for unmanned aerial vehicle: A review and comprehensive analysis," *Artificial Intelligence Review*, pp. 1–61, 2023.
- [28] E. Ristani and C. Tomasi, "Tracking multiple people online and in real time," in *Computer Vision—ACCV 2014: 12th Asian Conference on Computer Vision, Singapore, Singapore, November 1–5, 2014, Revised Selected Papers, Part V 12*. Springer, 2015, pp. 444–459.
- [29] M. Danelljan, G. Bhat, F. Shahbaz Khan, and M. Felsberg, "Eco: Efficient convolution operators for tracking," in *Proceedings of the IEEE conference on computer vision and pattern recognition*, 2017, pp. 6638–6646.
- [30] B. Li, J. Yan, W. Wu, Z. Zhu, and X. Hu, "High performance visual tracking with siamese region proposal network," in *Proceedings of the IEEE conference on computer vision and pattern recognition*, 2018, pp. 8971–8980.
- [31] N. Wang, W. Zhou, J. Wang, and H. Li, "Transformer meets tracker: Exploiting temporal context for robust visual tracking," in *Proceedings of the IEEE/CVF conference on computer vision and pattern recognition*, 2021, pp. 1571–1580.
- [32] H.-M. Hsu, J. Cai, Y. Wang, J.-N. Hwang, and K.-J. Kim, "Multi-target multi-camera tracking of vehicles using metadata-aided re-id and trajectory-based camera link model," *IEEE Transactions on Image Processing*, vol. 30, pp. 5198–5210, 2021.
- [33] Y. Cai and G. Medioni, "Exploring context information for inter-camera multiple target tracking," in *IEEE Winter Conference on Applications of Computer Vision*. IEEE, 2014, pp. 761–768.
- [34] H.-M. Hsu, T.-W. Huang, G. Wang, J. Cai, Z. Lei, and J.-N. Hwang, "Multi-camera tracking of vehicles based on deep features re-id and trajectory-based camera link models," in *CVPR workshops*, 2019, pp. 416–424.
- [35] Y.-G. Lee, Z. Tang, and J.-N. Hwang, "Online-learning-based human tracking across non-overlapping cameras," *IEEE Transactions on Circuits and Systems for Video Technology*, vol. 28, no. 10, pp. 2870–2883, 2017.
- [36] C. Ma, F. Yang, Y. Li, H. Jia, X. Xie, and W. Gao, "Deep trajectory post-processing and position projection for single & multiple camera multiple object tracking," *International Journal of Computer Vision*, vol. 129, pp. 3255–3278, 2021.
- [37] Z. Tang, G. Wang, H. Xiao, A. Zheng, and J.-N. Hwang, "Single-camera and inter-camera vehicle tracking and 3d speed estimation based on fusion of visual and semantic features," in *Proceedings of the IEEE conference on computer vision and pattern recognition workshops*, 2018, pp. 108–115.
- [38] Y. T. Tesfaye, E. Zemene, A. Prati, M. Pelillo, and M. Shah, "Multi-target tracking in multiple non-overlapping cameras using constrained dominant sets," *arXiv preprint arXiv:1706.06196*, 2017.
- [39] Y. Zhang, P. Sun, Y. Jiang, D. Yu, F. Weng, Z. Yuan, P. Luo, W. Liu, and X. Wang, "Bytetrack: Multi-object tracking by associating every detection box," in *European Conference on Computer Vision*. Springer, 2022, pp. 1–21.
- [40] X. Zhou, T. Yin, V. Koltun, and P. Krähenbühl, "Global tracking transformers," in *Proceedings of the IEEE/CVF Conference on Computer Vision and Pattern Recognition*, 2022, pp. 8771–8780.
- [41] K. G. Quach, P. Nguyen, H. Le, T.-D. Truong, C. N. Duong, M.-T. Tran, and K. Lu, "Dyglip: A dynamic graph model with link prediction for accurate multi-camera multiple object tracking," in *Proceedings of the IEEE/CVF Conference on Computer Vision and Pattern Recognition*, 2021, pp. 13 784–13 793.
- [42] Y. He, X. Wei, X. Hong, W. Shi, and Y. Gong, "Multi-target multi-camera tracking by tracklet-to-target assignment," *IEEE Transactions on Image Processing*, vol. 29, pp. 5191–5205, 2020.
- [43] Y. Gan, R. Han, L. Yin, W. Feng, and S. Wang, "Self-supervised multi-view multi-human association and tracking," in *Proceedings of the 29th ACM International Conference on Multimedia*, 2021, pp. 282–290.
- [44] Z. Liu, Y. Shang, T. Li, G. Chen, Y. Wang, Q. Hu, and P. Zhu, "Robust multi-drone multi-target tracking to resolve target occlusion: A benchmark," *IEEE Transactions on Multimedia*, 2023.
- [45] S. Hao, P. Liu, Y. Zhan, K. Jin, Z. Liu, M. Song, J.-N. Hwang, and G. Wang, "Divotrack: A novel dataset and baseline method for cross-view multi-object tracking in diverse open scenes," *International Journal of Computer Vision*, pp. 1–16, 2023.
- [46] Y.-J. Li, X. Weng, Y. Xu, and K. M. Kitani, "Visio-temporal attention for multi-camera multi-target association," in *Proceedings of the IEEE/CVF International Conference on Computer Vision*, 2021, pp. 9834–9844.
- [47] C.-C. Cheng, M.-X. Qiu, C.-K. Chiang, and S.-H. Lai, "Rest: A reconfigurable spatial-temporal graph model for multi-camera multi-object tracking," in *Proceedings of the IEEE/CVF International Conference on Computer Vision*, 2023, pp. 10051–10060.
- [48] F. Fleuret, J. Berclaz, R. Lengagne, and P. Fua, "Multicamera people tracking with a probabilistic occupancy map," *IEEE transactions on pattern analysis and machine intelligence*, vol. 30, no. 2, pp. 267–282, 2007.
- [49] Y. Xu, X. Liu, Y. Liu, and S.-C. Zhu, "Multi-view people tracking via hierarchical trajectory composition," in *Proceedings of the IEEE conference on computer vision and pattern recognition*, 2016, pp. 4256–4265.

- [50] T. Chavdarova, P. Baqué, S. Bouquet, A. Maksai, C. Jose, T. Bagautdinov, L. Lettry, P. Fua, L. Van Gool, and F. Fleuret, "Wildtrack: A multi-camera hd dataset for dense unscripted pedestrian detection," in *Proceedings of the IEEE conference on computer vision and pattern recognition*, 2018, pp. 5030–5039.
- [51] Y. Cui, C. Zeng, X. Zhao, Y. Yang, G. Wu, and L. Wang, "Sportsmot: A large multi-object tracking dataset in multiple sports scenes," *arXiv preprint arXiv:2304.05170*, 2023.
- [52] H. Zhao, J. Jia, and V. Koltun, "Exploring self-attention for image recognition," in *Proceedings of the IEEE/CVF conference on computer vision and pattern recognition*, 2020, pp. 10 076–10 085.
- [53] K. He, G. Gkioxari, P. Dollár, and R. Girshick, "Mask r-cnn," in *Proceedings of the IEEE international conference on computer vision*, 2017, pp. 2961–2969.
- [54] F. Yu, D. Wang, E. Shelhamer, and T. Darrell, "Deep layer aggregation," in *Proceedings of the IEEE conference on computer vision and pattern recognition*, 2018, pp. 2403–2412.
- [55] S. Shao, Z. Zhao, B. Li, T. Xiao, G. Yu, X. Zhang, and J. Sun, "Crowdhuman: A benchmark for detecting human in a crowd," *arXiv preprint arXiv:1805.00123*, 2018.
- [56] R. Han, W. Feng, J. Zhao, Z. Niu, Y. Zhang, L. Wan, and S. Wang, "Complementary-view multiple human tracking," in *Proceedings of the AAAI Conference on Artificial Intelligence*, vol. 34, no. 07, 2020, pp. 10 917–10 924.
- [57] K. Zhou, Y. Yang, A. Cavallaro, and T. Xiang, "Omni-scale feature learning for person re-identification," in *Proceedings of the IEEE/CVF international conference on computer vision*, 2019, pp. 3702–3712.
- [58] H. Luo, W. Jiang, Y. Gu, F. Liu, X. Liao, S. Lai, and J. Gu, "A strong baseline and batch normalization neck for deep person re-identification," *IEEE Transactions on Multimedia*, vol. 22, no. 10, pp. 2597–2609, 2019.
- [59] M. Ye, J. Shen, G. Lin, T. Xiang, L. Shao, and S. C. Hoi, "Deep learning for person re-identification: A survey and outlook," *IEEE transactions on pattern analysis and machine intelligence*, vol. 44, no. 6, pp. 2872–2893, 2021.



**Qiang Wang** received the Ph.D. degree in pattern recognition and intelligent systems from the University of Chinese Academy of Sciences, China, in 2020. He is currently a Research Associate with the Key Laboratory of Manufacturing Industrial Integrated Automation, Shenyang University. His research focuses on deep learning, multitask learning, feature selection, and image restoration.



**Baojie Fan** received the Ph.D. degree in pattern recognition and intelligent system from the State Key Laboratory of Robotics, Shenyang Institute Automation, Chinese Academy of Sciences. He is currently a Professor with the Department of Automation, NJUPT. His major research interests include robot vision systems, object detection, and tracking.



**Yandong Tang** received the B.S. and M.S. degree in the calculation of mathematics from Shandong University, China, in 1984 and 1987. From 1987 to 1996, he worked at the Institute of Computing Technology, Shenyang, Chinese Academy of Sciences. From 1996 to 1998, he was engaged in research and development at Stuttgart University and Potsdam University in Germany. He received a Ph.D. degree in Engineering Mathematics from the Research Center (ZETEM) of Bremen University, Germany, in 2002. From 2002 to 2004, he worked

at the Institute of Industrial Technology and Work Science (BIBA) at Bremen University of Germany. He is currently a Research Scientist with the Institute of Shenyang Automation of the Chinese Academy of Sciences. His research interests include image processing, mode recognition and robot vision.



**Huijie Fan** received the B.S. degree in automation from the University of Science and Technology of Science and Technology, China, in 2007, and the Ph.D. degree in mode recognition and intelligent systems from the Chinese Academy of Sciences University, China, in 2014. She is currently a Research Scientist with the Institute of Shenyang Automation of the Chinese Academy of Sciences. Her research interests include deep learning on image processing and medical image processing and applications.



**LianQing Liu** received his B.S. degree in Industry Automation from Zhengzhou University, Zhengzhou, China, in 2002, and his Ph.D. in Pattern Recognition and Intelligent Systems from Shenyang Institute of Automation, Chinese Academy of Sciences, Shenyang, China, in 2009. He is currently a professor at the Shenyang Institute of Automation, Chinese Academy of Sciences. His current research interests include nanorobotics, intelligent control, and biosensors.



**Tinghui Zhao** received the B.S. degree in automation from the Zhejiang University, China, in 2022. Currently he is a graduate student in Shenyang Institute of Automation, Chinese Academy of Sciences.